Ground Subsidence Response Conditional On Large-Scale Geothermal Exploitation In A Karst Reservoir Area of North China

Yahui Yao (yaoyahui@mail.cgs.gov.cn)
China University of Mining and Technology https://orcid.org/0000-0002-1125-6330
Xiaofeng Jia
China Geological Survey
Shengtao Li
China Geological Survey
Qiuxia Zhang
China Geological Survey
Jian Song
China Geological Survey
Hong Xiang
China Geological Survey
Junzhao Wang
China Geological Survey

Research Article

Keywords: Karst geothermal reservoir, Large-scale exploitation, Ground subsidence, Numerical simulation, North China

Posted Date: January 7th, 2022

DOI: https://doi.org/10.21203/rs.3.rs-1158021/v1

Ground subsidence response conditional on large-scale geothermal exploitation in a karst reservoir area of North China

Yahui Yao[1,2,3*], Xiaofeng Jia[2,3], Shengtao Li[2,3,4*], Qiuxia Zhang[2,3], Jian Song[2,3], Hong Xiang[2,3], Junzhao Wang[2]

[1] School of Resource and Earth Science, China University of Mining and Technology, Xuzhou, China;

[2] Center For Hydrogeology and Environmental Geology, China Geological Survey, Baoding, China；

[3] Technology Innovation Center of Geothermal & Hot Dry Rock Exploration and Development, MNR, Baoding, China；

[4] Technology Innovation Center for Geological Environment Monitoring Engineering, MNR, Baoding, China

*Correspondence:

yaoyahui@mail.cgs.gov.cn

list07@mails.jlu.edu.cn

Abstract

Carbonate karst geothermal resources are widely distributed and have large reserves in North China. Nowadays, the scale of exploitation and utilization of the carbonate karst geothermal resources is gradually increasing. In this work, a geothermal exploitation area where the karst geothermal reservoirs are exploited on a large scale, is selected as the study area, and methods including experiment and numerical simulation are used to study the exploitation-induced ground subsidence problems based on the long-term water level monitoring data of the geothermal reservoir. Through analyses of ground subsidence caused by water level change of the geothermal reservoir, the following conclusions were obtained. The water level drawdown of different types of geothermal reservoirs had different effects on ground subsidence. The maximum ground subsidence of the study area caused by the water level decline of the J*xw* carbonate geothermal reservoir was only 0.29 mm/a from 1983 to 2019, which is generally insignificant. In contrast, the same water level change of the N*m* sandstone geothermal reservoir was predicted to cause 8.9 mm/a ground subsidence. To slow down or even prevent the ground subsidence, balanced production and reinjection are required. From the result of this work, the decline of the water level of the J*xw* carbonate geothermal reservoir caused by current large-scale geothermal exploitation will not cause serious ground subsidence. However, attention should be paid to the N*m* sandstone type geothermal reservoirs as their structures are much more sensitive to the water pressure change.

Keywords Karst geothermal reservoir · Large-scale exploitation · Ground subsidence · Numerical simulation · North China

1. Introduction

Geothermal energy is a type of clean and renewable energy with strong competitiveness. The development and utilization of geothermal energy play an important role in clean heating in winter and haze treatment. Excessive exploitation of geothermal water can lead to the water level decline of the geothermal reservoir and ground subsidence (Zhang and Jin 1998; Hu et al. 2003; Parks et al. 2018; Liu et al. 2018; Eneva et al. 2020). At present, reinjection is an effective measure to alleviate the decline of water level and maintain the geothermal reservoir pressure (Duan et al. 2011). However, it is generally difficult to achieve the balance of production and reinjection, due to many factors such as geological conditions, technical level and so on.

With the increasing scale of geothermal development (Tian et al. 2020), more attention should be paid to the problem of ground subsidence caused by large-scale geothermal development. Recent studies have shown that exploitation of the sandstone porous geothermal reservoir has a certain contribution to ground subsidence (Li Hong et al. 2016; Ma Feng et al. 2021), but there is still a lack of quantitative research on whether the development of carbonate geothermal reservoir causes ground subsidence. The carbonate geothermal reservoir, known as the karst geothermal reservoir due to the existence of rock karstification to varying degrees, is a typical hydrothermal geothermal resource and is considered to be the most important thermal water resources outside of volcanic areas (Goldscheider et al. 2010). According to Pang et al. (2017), large karst geothermal reservoirs are developed in carbonate reservoirs widely distributed in North China, with excellent geothermal resource quality, large water volume, good water quality, high temperature and easy production and reinjection. It is the main area for the development and utilization of carbonate karst geothermal reservoirs in the middle of Bohai Bay Basin (Wang and Lin 2020), with a cumulative heating area of more than 40 million square meters (Wang et al. 2019). In this work, taking a concentrated production area of karst geothermal reservoir in North China as the study area, the objective is to evaluate the impact of karst reservoir pressure drop on ground

subsidence. The study is of significance to the sustainable development of geothermal resources and environmental protection.

2. Study area

2.1. Location

The study area is structurally located in the north-central of Jizhong Depression in Bohai Bay Basin(Fig. 1a), where the karst geothermal reservoir of Wumishan formation of Jixian system (Jx*w*) is taken as exploitation target. There are 20 geothermal wells in the study area, including 9 production wells and 11 reinjection wells. The distribution of geothermal wells is shown in Fig. 1b. The geothermal wells offer 63 ~ 78℃ hot water at about 100m^3/h flow rate. According to the statistics from 2014 to 2015, the annual production and reinjection volume of this area was 1903000 m^3 and the heating area was 1088000 m^2, which are categorized as the large-scale production and reinjection level.

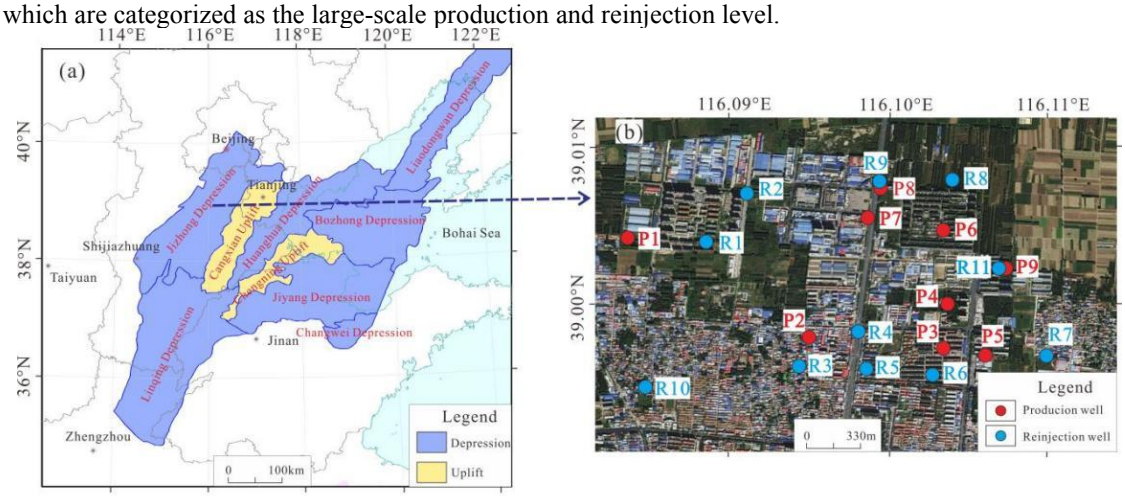

Fig. 1 Location of the study area and distribution of geothermal wells.

2.2. Geological and hydrogeological background

The stratum lithology encountered by drilling in the study area are clay and sandy clay in the Quaternary (Q), siltstone and mudstone in the Minghuazhen Formation of the Neogene system (N*m*), and dolomite in the Wumishan formation of Jixian system (Jx*w*). The geothermal reservoirs in the area include the sandstone geothermal reservoir of N*m* and the karst fissure geothermal reservoir of Jx*w*, among which the exploitation of N*m* reservoir is restricted by the government due to environmental protection. In the study area, the caprock is composed of Q and N*m* stratum, which has good thermal insulation and therefore is an ideal regional caprock. The N*m* is not only a geothermal reservoir but also a caprock of the underlying Jx*w*. Hot water in the karst reservoirs may be supplied by the lateral recharge and ascending deep fluids through transmissible pores and fractures or faults (Kong et al. 2017; Kong et al. 2020; Yao et al. 2020). According to the previous observation data of geothermal wells in the study area, the temperature, quantity and quality of the hot water are relatively stable, but the water level shows a downward trend year by year. Fig. 2 displays the conceptual model of reservoir engineering in the hydrothermal systems of the study area. The geothermal genesis model of the large-scale karst geothermal system is developed into a low-temperature convection-conduction geothermal system in a sedimentary basin (Wang et al. 2019; Pang et al. 2020).

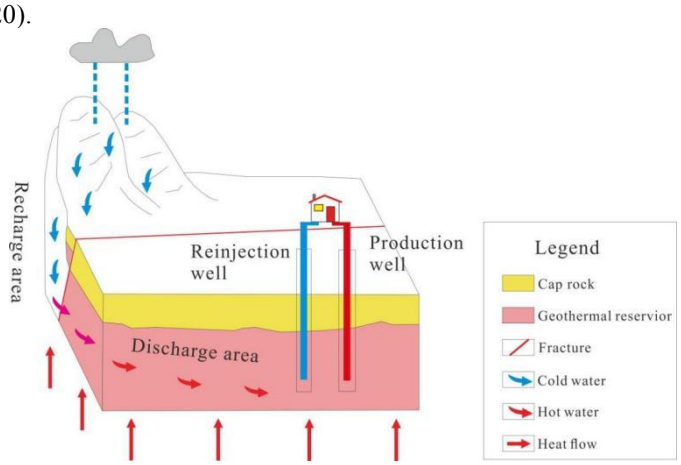

Fig. 2 The conceptual model of reservoir engineering in the hydrothermal systems of the study area (modified from Kong et al. 2014).

3. Material and methods

3.1. Coupling software and mathematical model

COMSOL is a large and advanced numerical simulation software, which is widely used in scientific research and engineering calculation in various fields, and can simulate various physical processes(Sheng et al.2017; Yue et al.2019). This study used the Poroelasticity multiphysics node of COMSOL, which includes the time rate of change in strain from the Solid Mechanics interface in the Darcy's Law interface and adds the fluid pressure gradient as stress contribution in the Solid Mechanics interface. The following sections describe the built-in equations when using the Poroelastic Material feature.

(1)Fluid flow

Use the Darcy's Law interface to estimate the flow field in the poroelastic model with the pressure head formulation

$$\rho_f S_\alpha \frac{\partial H}{\partial t} + \nabla \cdot \rho_f [-K \nabla H] = -\rho_f \alpha_B \frac{\partial}{\partial t} \varepsilon_{vol} \quad (1)$$

where ρ_f is the fluid density, H is the pressure head , K is the hydraulic conductivity, ε_{vol} is the volumetric strain of the porous matrix, α_B is the Biot coefficient and S_α is Poroelastic storage coefficient.

(2)Porous matrix deformation

The governing equation for the poroelastic material model is

$$-\nabla \cdot \sigma = \rho g \quad (2)$$

Where σ is the stress tensor, ρ is the total density, and g is acceleration of gravity. The poroelastic material model uses Equation 2 to describe changes in the stress tensor σ and porous matrix displacement u due to boundary conditions and changes in pore pressure.

3.2. 3D geological model

The strata data exposed by the 20 geothermal wells in the study area are shown in Table 1, whose formations are Q, N*m* and Jx*w*. The stratum structure is simple, and the fault structure is not developed. Among the wells, the maximum vertical thickness of Jx*w* exposed by well P8 is 762.5m. Considering that the stratum thickness of Jx*w* is about 1400~1500m in the study area, and the maximum drilling depth of the 20 geothermal wells is 1717.54m, it is speculated that the stratum at the 2000m depth of the study area is Jx*w*. In view of the accuracy of the 3D geological model and the efficiency of later numerical calculation, the strata at a depth of 2000m was selected as the bottom boundary to establish the 3D geological model. According to the stratum information of 20 geothermal wells in the study area, the depth and thickness data of each layer were obtained through interpolation (As shown in Fig. 3). The 3D geological model was established according to the stratum structure from the ground surface to 2000 m below (Fig. 4), whose horizontal boundary was determined according to the scope of the study area. The model was divided into 49138 calculation mesh cells. On the premise of reflecting the original geological conditions as much as possible, some assumptions and simplification were adopted for the model geological conditions. Specifically, only the gravity was considered for the original stress field, and each rock or soil layer was treated as a uniform continuous medium. For the Jx*w* geothermal reservoir, according to the logging interpretation results and reservoir characteristic parameters of P4 well (Table 2), its fracture development section and dense section are distributed alternatively, and the reservoir thickness ratio is 32.62%. Considering the large differences in physical and mechanical properties between the fractures development section and the dense section of Jx*w* geothermal reservoir and the difficulties to establish a geological model consistent with the real reservoir due to the complex development and distribution of fractures in Jx*w* geothermal reservoir, the 3D geological model of Jx*w* exposed at a shallow depth of 2000m was simplified into two parts, which are karst fractures development section (Jx*w*-1) and dense section (Jx*w*-2) according to the reservoir thickness ratio parameter.

Table 1 List of strata data exposed by 20 geothermal wells in the study area.

Well type	Well number	Well depth (m)	Bottom boundary depth of stratum (m)			Exposed stratum thickness (m)		
			Q	N*m*	Jx*w*	Q	N*m*	Jx*w*
producing well	P1	1580	364.52	850	1580	364.52	485.48	730
	P2	1301	390.3	990	1301	390.3	599.7	311
	P3	1286	312.5	1042	1286	312.5	729.5	244

	P4	1600	402	1070	1600	402	668	530
	P5	1506.4	405	1072	1506.4	405	667	434.4
	P6	1250	397.7	1065	1250	397.7	667.3	185
	P7	1506	305.3	930.43	1506	305.3	625.13	575.57
	P8	1693.5	322	931	1693.5	322	609	762.5
	P9	1500	405	1052	1500	405	647	448
Reinjection well	R1	1068.93	332.5	932.3	1068.93	332.5	599.8	136.63
	R2	1500	299.9	990.35	1500	299.9	690.45	509.65
	R3	1028	400	999	1028	400	599	29
	R4	1070	390.5	1011	1070	390.5	620.5	59
	R5	1201.8	392	1030	1201.8	392	638	171.8
	R6	1284.57	398.5	1085	1284.57	398.5	686.5	199.57
	R7	1501.01	398	1043.2	1501.01	398	645.2	457.81
	R8	1500	419.44	992.11	1500	419.44	572.67	507.89
	R9	1506	318.5	948.05	1506	318.5	629.55	557.95
	R10	1500	425.25	980.26	1500	425.25	555.01	519.74
	R11	1717.54	403.69	1268.3	1717.54	403.69	864.61	449.24

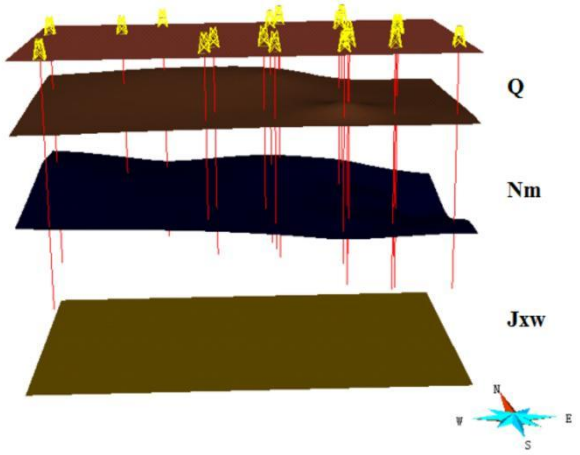

Fig. 3 Schematic diagram of strata and geothermal wells in the study area.

Table 2 Characteristic parameters of J*xw* geothermal reservoir of P4 well.

Geothermal well	Exposed thickness (m)	Reservoir thickness ratio (%)	Crack rate (%)	Permeability (mD)	Water flow rate (m^3/h)	Water flow rate per unit thickness ($m^3/(h \cdot m)$)	Water temperature (℃)
P4 well	172.89	32.62	4.89	2.2	135.6	20.67	65

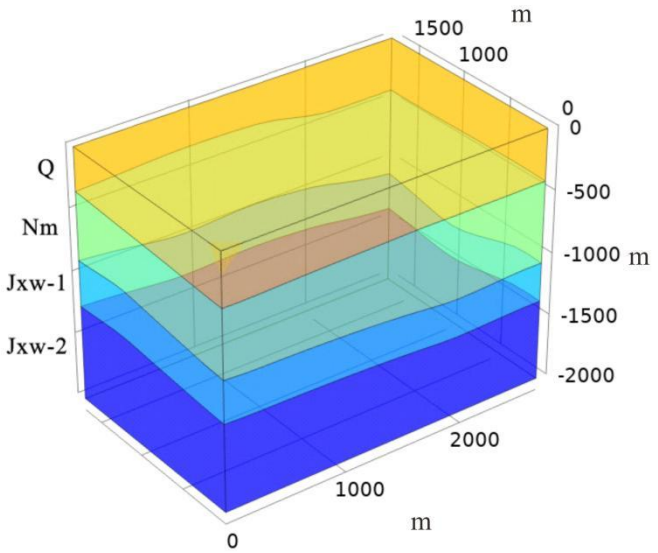

Fig. 4 3D geological model of the study area.

3.3. Setting of boundary conditions and initial conditions

The hydrogeological boundary conditions of the 3D model are described as follows. The horizontal direction of the model is considered as an infinite recharge boundary. The Jxw geothermal reservoir is in direct contact with the Nm vertically, and the thick mudstone at the bottom of the Nm, which plays a role in blocking water, directly covers the Jxw geothermal reservoir. Therefore, the upper surface of the Jx*w* is treated as a water barrier boundary. There is no water blocking boundary in the lower part of the Jx*w*, so the bottom boundary is an infinite recharge boundary. The mechanical boundary conditions of the 3D model are described as follows. The lateral sides of the model are restrained in the horizontal direction. The bottom boundary is restrained in both vertical and horizontal directions, and the top of the model is a free boundary.

The deformation calculation initiates at the initial water level, and it is assumed that the vertical displacement of all points at this time is 0. A positive deformation value indicates subsidence, and a negative deformation value indicates uplift.

3.4. Experiment and model parameter acquisition

The rock mechanical parameters of Jx*w* geothermal reservoir were confirmed by the triaxial compression test. The rock samples of Jx*w* were taken from the outcrop in the mountain area near the study area. The RMT-150C rock mechanics measuring system was applied in the Institute of Rock and Soil mechanics, Chinese Academy of Sciences. From the triaxial compression test results (Table 3) and the stress strain curves (Fig. 5), the triaxial compressive strength and elastic modulus of the rock samples basically increase with the increase of confining pressure. The triaxial compressive strength of rock samples ranges from 341.753 to 507.428 Mpa, and the elastic modulus ranges from 46.951 to 52.793 Gpa. The main physical and mechanical parameters for each stratum of the 3D model are shown in Table 4. Due to the complex fracture structure development of carbonate geothermal reservoir, it is difficult to obtain the Biot coefficient reflecting the real reservoir through the experimental test. The Biot coefficient of Jx*w*-1 and N*m* were referred to Bai (2016). The elasticity modulus of Jx*w*-2 was determined using the above test results. Since it is difficult to obtain the elastic modulus of the fractured section of the Jx*w* reservoir, the elasticity modulus of Jx*w*-1 was estimated as 40% of the Jx*w*-2. The elasticity modulus of Q and N*m* were referred to the Ma et al. (2016).

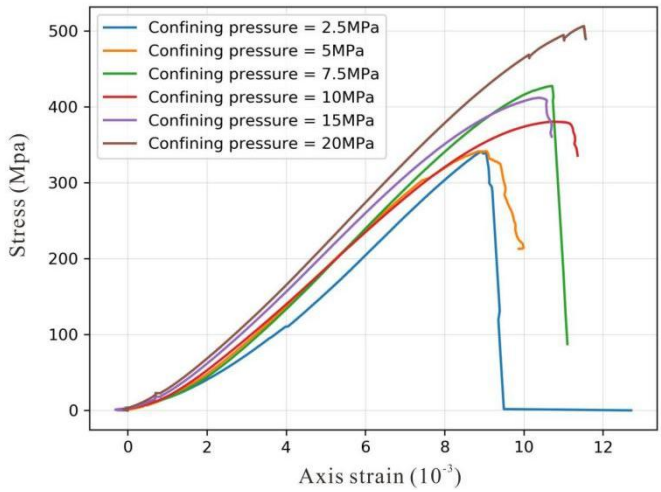

Fig. 5 Stress-strain curve of triaxial compression test

Table 3 Triaxial compression test results.

Rock mechanical parameters	Sample 1	Sample 2	Sample 3	Sample 4	Sample 5	Sample 6
Confining pressure （MPa）	5.0	10.0	15.0	2.481	7.501	20
Compressive strength （MPa）	342.615	380.962	412.960	341.753	428.439	507.428
Elastic modulus （GPa）	49.784	46.951	51.137	47.111	52.793	53.837

Table 4 Physical and mechanical parameters for each stratum of the 3D model

Stratum	Density （kg/m^3）	Elastic modulus (MPa)	Poisson's ratio	Biot coefficient	Porosity	permeability （mD）
Q	2000	500	0.35	—	—	—
N*m*	2300	1500	0.3	0.8	0.1	1
Jx*w*-1	2600	20000	0.27	0.6	0.05	2.2
Jx*w*-2	2800	50000	0.25	—	—	—

4. Results and discussion

Firstly, this study simulated the ground subsidence response under the condition of large-scale development of Jx*w* karst geothermal reservoir from 1983 to 2020, based on the long-term water level monitoring data of the X101 and D02 well before heating season in November every year. The X101 well, a water level observation station of the Jx*w* reservoir located about 2 km to the south of the study area, recorded the water level data in 1983 and the period from 2000 to 2014. The D02 well, another water level observation station of the Jx*w* reservoir located about 8 km to the nouth of the study area, continuously recorded the water level data from 2019 to 2020. The long-term water level monitoring data are shown in Figure 6. It should be noted that the local government banned a number of illegal geothermal wells and strengthened the management measures of balanced geothermal production and reinjection from 2019, causing the water level in the same period in 2020 is higher than that in 2019. The exploitation of the Nm geothermal reservoir in the study area has been forbidden. However, in order to compare and study the impact of water level drop of N*m* semi-consolidated sandstone geothermal reservoir on ground subsidence, the simulations considering different water level drawdown scenarios were also carried out for N*m* reservoir. The water level monitoring data of the Jxw reservoir were also adopted in the simulation of the Nm reservoir. The simulation results of maximum surface deformation caused by different water level drawdown of Jx*w* and N*m* geothermal reservoirs are shown in Table 5 and Figure 6.

4.1. Jx*w* geothermal reservoir

According to the simulation results (Table 5, Figure 6 and Figure 7), the water level drawdown of the Jxw geothermal reservoir has little effect on the ground subsidence. From 1983 to 2019, the water level decreased from -0.75 m to -117 m, with the water level decline rate reaching 3.23 m/a, which only caused maximum ground subsidence of 10.5 mm and average annual ground subsidence of 0.29 mm/a. Particularly, from 2000 to 2019, due to the increase of geothermal exploitation, the water level decreased from -35.8m to -117m, and the water level decline rate reached 4.27 m/a. The maximum ground subsidence caused in the period was 7.3 mm, with average annual ground subsidence of 0.38mm/a. In this work, we divided this period into the following five stages:

From 2000 to 2006 was the stage of slow increase of the geothermal production, the water level decreased from -35.8 m to -43.7 m, and the water level decline rate was 1.3 m/a. The caused maximum ground subsidence was 0.7 mm, and the average annual ground subsidence was 0.12 mm/a. The period from 2006 to 2010 saw a rapid increase of the geothermal production, when the water level decreased from -43.7 m to -70.4 m (6.7 m/a) and caused 2.4 mm maximum ground subsidence (0.6mm/a). From 2010 to 2013, due to the start of the reinjection project, the decline rate of water level slowed down. The water level dropped from -70.4 m to -87.9 m, and the water level drop rate reduced to 5.8 m/a. The total ground subsidence caused in these three years was 1.6 mm (0.53 mm/a). From 2014 to 2019, the water level still showed a downward trend. However, due to the lack of monitoring data from 2014 to 2018, we only analyze the data of 2019 here. In the year 2019, the water level dropped to -117m, and the total land subsidence was 10.5mm. 2019 to 2020 is the last stage, during which a large number of geothermal wells around the study area were shut down, causing the water level to rise from − 117 m to − 114 m and the land subsidence to rebound by 0.3 mm.

The above data conclude that the subsidence caused by the water level drop of the carbonate geothermal reservoir of Jx*w* is generally insignificant. Because the carbonate geothermal reservoir results from elastic deformation, the rebound deformation occurs when the water level rises. If the production and reinjection are balanced and the water level remains unchanged, the ground subsidence is not likely to increase. The karst fractures development section of Jx*w*-1 in the upper part of Jx*w* is the main thermal water exploitation section. The effective stress change caused by the change of water level mainly acts on the Jx*w*-1 section, resulting in the deformation of geothermal reservoir structure.

4.2. N*m* geothermal reservoir

According to the simulation results (Table 5, Fig. 6 and Fig. 8), with the annual increase of water level drawdown of N*m*, the ground subsidence was observed. From 1983 to 2019, the water level decreased from -0.75m to -117m, resulting in a maximum ground subsidence of 320.5 mm and an average annual subsidence of 8.9 mm/a. From 2000 to 2019, the geothermal production increased sharply, and the water level decreased from -35.2 m to -117 m. The maximum ground subsidence caused was 223.7 mm, and the average annual ground subsidence was 11.78 mm/a. Because the N*m* sandstone geothermal reservoir is a semi-consolidated formation, the effective stress change caused by the change of water level has a large deformation on the geothermal reservoir structure.

According to Li et al. (2016), the average annual ground subsidence caused by the development of N*m* geothermal reservoir was 8.52mm/a in Tanggu District, Tianjin City, which is close to the simulation results of the study and can explain the rationality of the simulation results.

Table 5 Statistics of simulation results of maximum surface deformation caused by different water level drawdown of Jx*w* and N*m* geothermal reservoirs.

Number	Year	Water level（m）	Drawdown（m）	Maximum ground subsidence caused by water level drop（mm）		Annual average value of maximum ground subsidence caused by water level drop（mm/a）	
				Jx*w*	N*m*	Jx*w*	N*m*
1	1983	-0.75	0	0	0		
2	2000	-35.8	35.05	3.2	96.8		
3	2001	-38.6	37.85	3.4	104.5		
4	2002	-39.6	38.85	3.5	107.3	0.12	3.6
5	2003	-41.4	40.65	3.7	112.2	（2000-2006）	（2000-2006）
6	2004	-41.4	40.65	3.7	112.2		
7	2005	-42.2	41.45	3.8	114.4		
8	2006	-43.7	42.95	3.9	118.3		
9	2007	-53.3	52.55	4.7	145.2		
10	2008	-58.9	58.15	5.3	160.6	0.6	18.4
11	2009	-66.5	65.75	5.9	181.5	（2006-2010）	（2006-2010）
12	2010	-70.4	69.65	6.3	191.9		
13	2011	-72.7	71.95	6.5	198.5		
14	2012	-77.3	76.55	6.9	211.1	0.53	16.1
15	2013	-87.9	87.15	7.9	240.3	（2010-2013）	（2010-2013）
16	2019	-117.0	116.25	10.5	320.5	-0.3	-8.3
17	2020	-114.0	113.25	10.2	312.2	（2019-2020）	（2019-2020）

Note: Taking the water level in 1983 as the initial state, it is assumed that the vertical displacement in this state is 0.

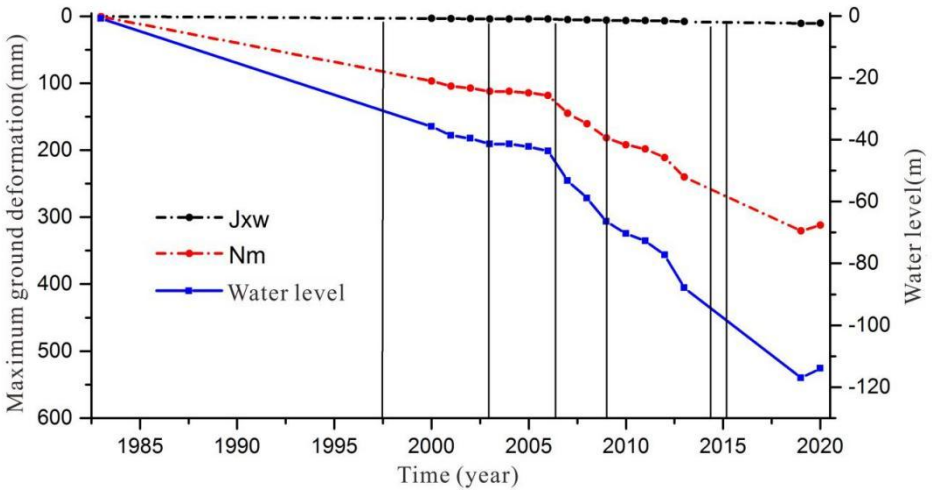

Fig. 6 Simulation results of maximum ground subsidence corresponding to the water level of Jx*w* and N*m* geothermal reservoirs in different years

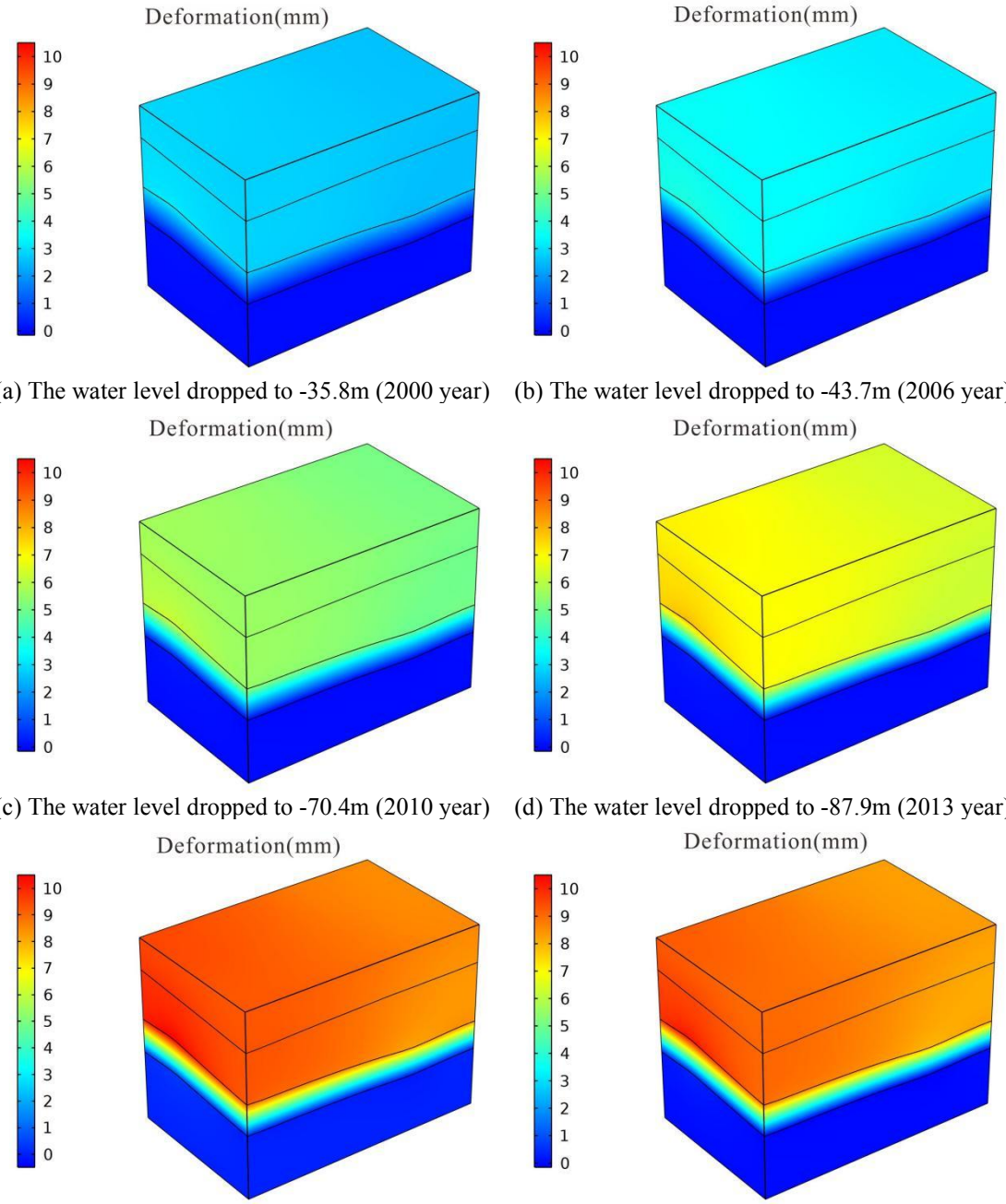

(a) The water level dropped to -35.8m (2000 year) (b) The water level dropped to -43.7m (2006 year)

(c) The water level dropped to -70.4m (2010 year) (d) The water level dropped to -87.9m (2013 year)

(e) The water level dropped to -117m (2019 year) (f) The water level dropped to -114m (2020 year)

Fig. 7 Distribution of deformation caused by water level falling from -0.75m to different depths of J*xw*

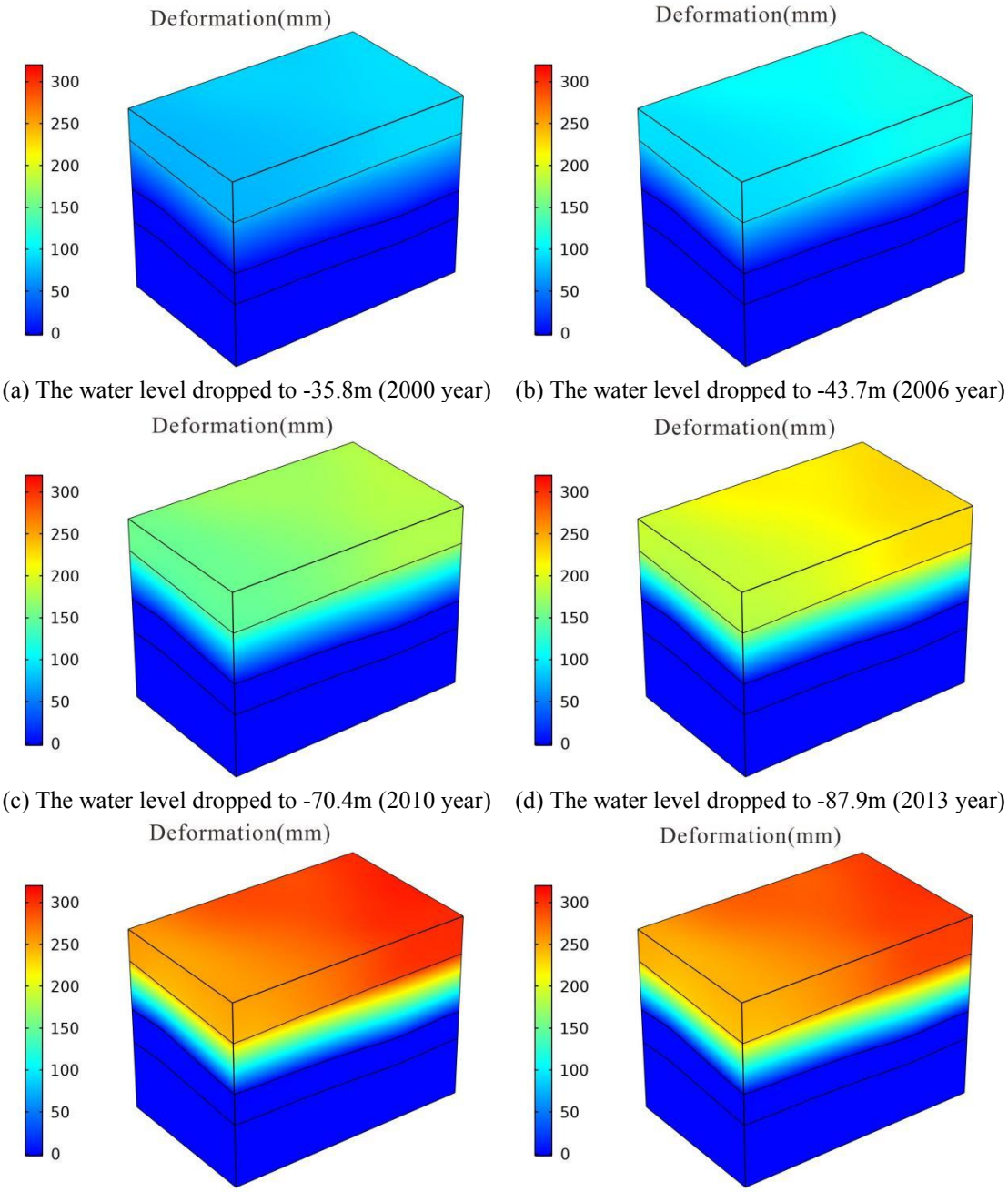

(a) The water level dropped to -35.8m (2000 year) (b) The water level dropped to -43.7m (2006 year)

(c) The water level dropped to -70.4m (2010 year) (d) The water level dropped to -87.9m (2013 year)

(e) The water level dropped to -117m (2019 year) (f) The water level dropped to -114m (2020 year)

Fig. 8 Distribution of deformation caused by water level falling from -0.75m to different depths of N*m*.

4.3. Analysis

From the simulation results, the water level drawdown of Jx*w* carbonate reservoir and N*m* sandstone reservoir showed an obvious linear correlation with the maximum ground subsidence. With the increase of water level drawdown, the ground subsidence also increases. For a given water level drop, the maximum ground subsidence caused by N*m* sandstone geothermal reservoir is nearly 30 times that of Jx*w* carbonate reservoir, indicating that ground subsidence is much more sensitive to the water level change of the Nm sandstone geothermal reservoir than that of the Jxw carbonate geothermal reservoir. The main reason for this phenomenon is the difference of rock consolidation characteristics and mechanical properties between the two types of geothermal reservoirs. The Jx*w* carbonate geothermal reservoir is fully consolidated rock with stable mechanical properties. In contrast, the semi-consolidated rock stratum of N*m* sandstone reservoir has poor mechanical properties. The change of fluid pressure will increase the effective stress of the reservoir. The pressure increment of the reservoir structure caused by the same

water level change is consistent, but the difference of ground subsidence caused is huge due to the difference of key influencing parameters such as elastic modulus and Biot coefficient.

5. Conclusion

The ground subsidence of the study area was mainly caused by the exploitation of geothermal resources and groundwater (Zhang et al. 2018). The ground subsidence caused by groundwater exploitation in Quaternary strata has been widely recognized (Yang et al. 2013). There are few studies focusing on ground subsidence caused by geothermal reservoir exploitation. By comparing and analyzing the response relationship between ground subsidence and water level change of geothermal reservoir in the study area, the following conclusions were obtained.

The water level drawdown of different types of geothermal reservoirs had different effects on the ground subsidence. From 1983 to 2019, the ground subsidence caused by the water level decline of J*xw* carbonate geothermal reservoir in the study area was only 0.29mm/a, which is insignificant. In contrast, the same water level drop of the Nm sandstone geothermal reservoir was predicted to cause 8.9 mm/a ground subsidence. Under the condition of balanced production and reinjection, controlling the water level decline rate of geothermal reservoir can effectively slow down and even prevent ground subsidence. Due to the control of internal factors such as mechanical properties and structural characteristics of geothermal reservoir, the ground subsidence caused by J*xw* carbonate geothermal reservoir with good consolidation and strong deformation resistance is much less than that of semi-consolidated N*m* sandstone geothermal reservoir under the same water level drawdown condition. The structural deformation of J*xw* carbonate geothermal reservoir in the study area is not sensitive to water level decline. Under the current large-scale geothermal exploitation conditions, the water level decline of the J*xw* carbonate geothermal reservoir will not cause serious ground subsidence. However, attention should be paid to the Nm sandstone geothermal reservoir as their structures are much more sensitive to the water pressure change.

Acknowledgements The research work was funded by the National Key Research and Development Program (No.2018YFC0604305) and the Project of China Geological Survey (No.DD20190127).

Declarations

Conflict of interest The authors declare that they have no potential conflicts of interest with respect to the research, authorship, and publication of this article.

References

Bai L (2016) Experimental analysis of rock Biot coefficient and engineering application of geological disposal of carbon dioxide. MSc Thesis. Jilin University (in Chinese)

Duan Z, Pang Z, Wang X (2011) Sustainability evaluation of limestone geothermal reservoirs with extended production histories in Beijing and Tianjin, China. Geothermics 40(2): 125-135. doi: 10.1016/j.geothermics.2011.02.001

Eneva M, Adams D, Blake K, Hsiao V, Falorni G (2020) Comparison of Surface Deformation Rates from InSAR and Ground-Based Surveys in Geothermal Fields of California. PROCEEDINGS, 45th Workshop on Geothermal Reservoir Engineering Stanford University, Stanford, California

Goldscheider N, Mádl-Szőnyi J, Erőss& A, Schill E (2010) Review: Thermal water resources in carbonate rock aquifers. Hydrogeology Journal 18(6):1303-1318. doi: 10.1007/s10040-010-0611-3

Hu X, Sun J, Yao Z, Rong F (2003) Research on the influence of geothermal activities and exploitation to geological environment in Tibet. Journal of Mountain Science (S1): 45-48 (in Chinese)

Kong Y L, Pang Z H, Pang J M, li J, Lyu Min (2020) Fault-Affected Fluid Circulation Revealed by Hydrochemistry and Isotopes in a Large-Scale Utilized Geothermal Reservoir. Geofluids 24: 1-13. doi: 10.1155/2020/2604025

Kong Y L, Pang Z H, Pang J M, Wang Y, Yang F. (2017) Stable isotopes of deep groundwater in the Xiongxian geothermal field. Procedia Earth & Planetary Science 17: 512-515. doi: 10.1016/j.proeps.2016.12.129

Kong Y, Pang Z, Shao H, Hu S, Kolditz O (2014) Recent studies on hydrothermal systems in China: a review. Geothermal Energy (2): 1-12. doi: 10.1186/s40517-014-0019-8

Li H, Xiao G, Yang J, Zhao g, Xiao Y (2016) Precise identification of land-subsiding layers and reconstruction of subsid-ence process in Tianjin Binhai New Area. Geological Bulletin of China 35(10): 1646-1652 (in Chinese)

Liu F, Fu P, Mellors RJ, Plummer MA, Ali ST et al. (2018) Inferring Geothermal Reservoir Processes at the Raft River Geothermal Field, Idaho, USA, Through Modeling InSAR-Measured Surface Deformation. Journal of Geophysical Research: Solid Earth 132(7): 1-34. doi: 10.1029/2017JB015223

Ma F, Wang G, Zhang W, Zhu X, Zhang H, et al. (2021) Study on the influence mechanism of the ancient buried hill geothermal exploitation on land subsidence. Geology in China 48(1): 40-51 (in Chinese)

Ma S, Wang X, Ma X, Cao X (2016) Experimental study on mechanical characters of Neogene weak cementation rock. Yellow River 38(5): 121-124 (in Chinese)
Pang Z, Kong Y, Pang J, Hu S, Wang J (2017) Geothermal resources and development in Xiongan New Area. Bulletin of Chinese Academy of Sciences 32(11): 1224-1230 (in Chinese)
Pang Z, Pang J, Kong Y, Guo S, Wang S, et al. (2020) Large-scale karst thermal storage identification method and large-scale sustainable mining technology. Science and Technology for Development 16(3): 299-306. doi: 10.11842/chips.20200516001 (in Chinese)
Parks M, Sigmundsson F, Sigurðsson Ómar, Hooper A, Hreinsdóttir Sigrún, et al. (2018) Deformation due to geothermal exploitation at Reykjanes, Iceland. Journal of Volcanology and Geothermal Research 391: 1-12. doi: 10.1016/j.jvolgeores.2018.08.016
Sheng D, Lv Y, Zhou Z (2017) Numerical Simulation of Land Subsidence Mine Water Area. Coal Technology 36(11): 187-189 (in Chinese)
Tian T, Dong Y, Zhang W, Wei J, Jin H, et al. (2020) Rapid Development of China's Geothermal Industry - China National Report of the 2020 World Geothermal Conference. Proceedings World Geothermal Congress 2020, Reykjavik, Iceland
Wang G, Lin W (2020) Main hydro-geothermal systems and their genetic models in China. Acta Geologica Sinica 94(7): 1923-1937 (in Chinese)
Wang X, Mao X, Ji L, Liu H, Luo L, et al. (2019) Karst Geothermal System in the Beijing-Tianjin-Hebei Plain of North China. PROCEEDINGS, 44th Workshop on Geothermal Reservoir Engineering, Stanford University, Stanford, California
Wang Z, Zhang C, Jiang G, Hu J, Tang X, et al. (2019) Present-day geothermal field of Xiongan New Area and its heat source mechanism. Chinese Journal of Geophysics 62(11): 4313-4322. doi: 10.6038/cjg2019M0326 (in Chinese)
Yang Y, Zheng F, Liu L, Dou Y, Jia S (2013) Susceptibility zoning and control measures on land subsidence caused by groundwater exploitation. Geology In China 40(2): 653-658 (in Chinese)
Yao Y, Jia X, Li S, Zhang J, Song J, et al. (2020) Study on heat flow determination from Archean under the karst thermal reservoir of D01 well in Xiongan New Area Geology In China : 1-11. http://kns.cnki.net/kcms/detail/11.1167.P.20201207.1546.002.html (in Chinese)
Yue G, Wang G, Ma F, Zhang W, Yang Z (2019) The thermal state and geothermal energy accumulation mechanism in the xiong'an new area, china. Energy Exploration & Exploitation 37(3): 1039-1052. doi: 10.1177/0144598719840741
Zhang B, Jin A (1998) Effect of extracting geothermal resources on land subsidence in Binhai Area of Tianjin city. The Chinese Journal of Geological Hazard and Control 9(2): 112-117 (in Chinese)
Zhang Y, Liu B, Wu H, Cheng X, Kang Y (2018) Ground subsidence in Xiong′an New Area from 2012 to 2016 Monitored by InSAR technique. Journal of Earth Science and Environment 40(5): 652-662 (in Chinese)